

# A novel dual-leg DC-DC converter for wide range DC-AC conversion

K. Suresh & E. Parimalasundar

To cite this article: K. Suresh & E. Parimalasundar (2022) A novel dual-leg DC-DC converter for wide range DC-AC conversion, *Automatika*, 63:3, 572-579, DOI: [10.1080/00051144.2022.2056809](https://doi.org/10.1080/00051144.2022.2056809)

To link to this article: <https://doi.org/10.1080/00051144.2022.2056809>



© 2022 The Author(s). Published by Informa UK Limited, trading as Taylor & Francis Group.



Published online: 30 Mar 2022.



Submit your article to this journal [↗](#)



Article views: 465



View related articles [↗](#)



View Crossmark data [↗](#)



# A novel dual-leg DC-DC converter for wide range DC-AC conversion

K. Suresh and E. Parimalasundar

Department of EEE, Sree Vidyanikethan Engineering College, Tirupati, Andhra Pradesh, India

## ABSTRACT

This paper proposes DC-AC Dual-leg dual-stage Conversion (DDC) and DC-AC Direct single-stage conversions (DSC). Conventional energy conversion system has only two-stage conversion, so it has some drawbacks such as huge power loss, less conversion range and lower power rating. So direct conversion, dual-leg step-up and step-down conversions are the solutions to get wide voltage conversion efficiently. The proposed converter can perform the power conversion from battery DC supply into AC with 1:1 ratio, step-up AC, and step-down AC in both directions. Also, it can perform rectifier operation from grid AC supply into DC with 1:1 ratio, step-down DC, and step-up DC. Step-up, step-down and ideal operations are possible within a single circuit; its operation is similar to solid-state DC-AC/AC-DC transformer. The ideal operation, Step-down to Step-up conversion and Step-up to Step-down conversion are possible on both sides, so this converter can handle a wide range of voltage. Power distribution is achieved with voltage regulation between battery/DC-load and AC-load/grid using the proposed control strategy with proper modulation. A prototype model of a 2-kW power rating validates the advantages and feasibility of the proposed methodology.

## ARTICLE HISTORY

Received 16 May 2021  
Accepted 15 March 2022

## KEYWORDS

Boost inverter; boost rectifier; ideal inverter; ideal rectifier; buck inverter; buck rectifier

## 1. Introduction

Renewable energy-based modern electric vehicle micro-grid and other power systems demand converter operation with flexible conversions range. Energy storage in an electrical system is important to avoid power failure and make unstable natural energies into constant levels. The energy storage system is an important part in efficiency and stability, energy from renewable sources and effective utilization is the bidirectional power flow operations. DC-DC and DC-AC bidirectional converters are connected, which composed a dual-stage structure, it can be useful for light-load applications in industry, and it can be controlled by Pulse Width Modulation (PWM). Modelling and analyzing PWM control in a controller are also important tasks [1,2]. DC-DC converter controlled by PI (Proportional-Integral) controller-based nested loop is for closed-loop operation, and the operation is analyzed with transfer function or small-signal modelling. This conversion may be step-up/step-down, but the conversion range should be high with minimum voltage stress [3,4]. Plenty of DC-DC converter topologies are available for chopper operation are flyback, forward, etc., among these suitable selections, DC-DC converter topology is important. Some of the applications demand multistage DC-DC conversion, so cascaded operation is required with proper feedback [5,6]. While performing step-up/step-down operations, voltage gain is an important parameter; it should always

be high; accordingly, modified converter topologies are important [5,7]. Modern converter topologies demand different control strategies while performing a bidirectional operation, i.e. grid to a battery (AC to DC) and vice versa. During this conversion, soft switching and ripple-free output are required to enhance efficiency. Conversion of the power from one form to the required form, phase lead FIR filters are also helpful to minimize output ripples [8,9]. Advanced PWM techniques help perform operations like high-frequency link clamping operations and achieve accurate unity power factor [10–12]. Some HVDC applications demand matrix types or multilevel operations with soft switching to improve output quality by reducing Total Harmonic Distortion (THD) [13–15]. From the literature, a novel DC-AC converter is presented that can perform a freewheeling operation using feedback power diodes; it can suppress leakage current in a common state, which is suitable for PV-based grid applications [12]. Active-switched T-source boost inverter, active-switched-source boost inverter, flipped active-switched-source boost inverter, and active switched Y-source boost inverter are all examples of active-switched boost inverters. The asymmetrical tri-state bidirectional inverter (ASTS-BI) demonstrates the suggested converter's operating concept, steady-state analysis and parameter design, and feature comparisons for the four topologies offered [16]. All of the suggested ANPC inverters were thoroughly investigated

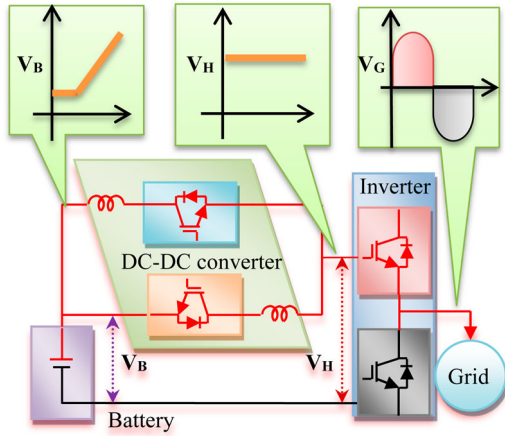


Figure 1. The existing system (cascaded).

and tested. Their operations were verified, and the experimental and theoretical findings were in good accord [17]. This letter proposes a new five-level ANPC inverter. The suggested architecture inherits the traditional ANPC inverter’s capacity to mitigate high-frequency CMV while also providing additional benefits such as voltage-boosting, improved dc-link voltage consumption, decreased voltage stress, and increased compactness [18]. Conventional converters have a disadvantage with more number conversion stages; application-oriented topology design is the solution for any type of conversion issue. The proposed converter can perform direct conversion, Step-down to Step-up conversion and Step-up to Step-down conversion from the battery to the inverter, vice versa conversions with various voltages, similar to transformer operation.

**2. Proposed DC-DC converter circuit analysis**

The proposed power conversion system is divided into six modes of operation; the main advantages of this proposed system are flexible conversion operation, power loss reduction, and high power rating in single-phase operation. Overall operation is classified into three groups: direct conversion, two-stage Step-up to Step-down conversions, and two-stage Step-down to Step-up conversions (Figures 1–4).

From the classified group of conversion, each group can perform rectifier and inverter operations.

**2.1. Direct rectifier operation**

Direct rectifier operation involves horizontal switches (diode anti-parallel to switches  $S_{H1}$  and  $S_{H3}$  are forward biased and  $S_{H2}$  &  $S_{H4}$  are ON) and vertical switches (diode anti-parallel to negative switches  $S_{N1}$  and  $S_{N2}$  are forward-biased). So the alternating current from source  $V_{AC}$  is converted into  $V_{DC}$  in the ratio of 1:1, which is given to the battery. Average output voltage during rectification mode with R load is expressed in Equation (1)

$$V_{DCavg} = \frac{2V_m}{\pi} \cos\alpha \tag{1}$$

$$V_{DCrms} = \frac{V_m}{\sqrt{2}} \tag{2}$$

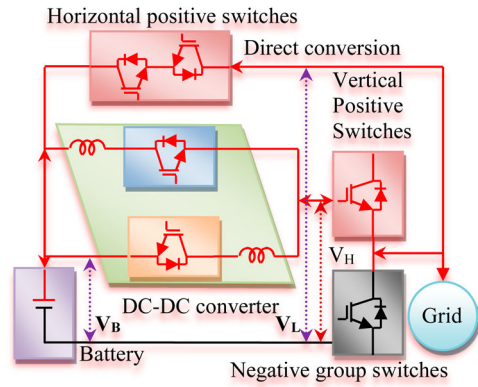


Figure 2. The proposed system.

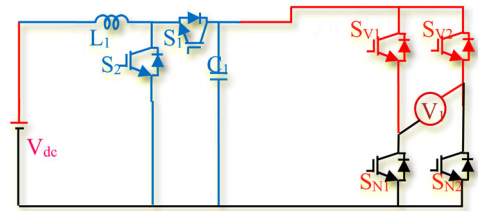


Figure 3. The existing circuit.

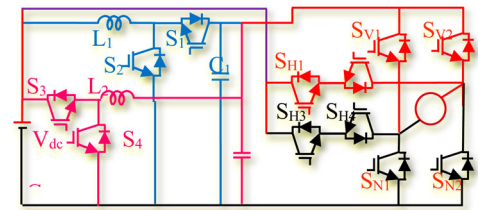


Figure 4. Proposed circuits.

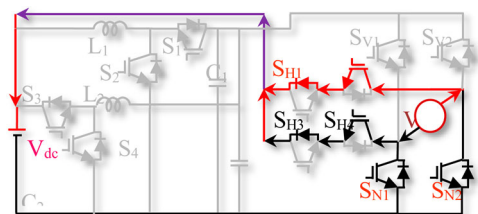


Figure 5. Direct rectification.

(Figure 5)

**2.2. Direct inverter operation**

Direct inverter operation also involves horizontal switches (diode anti-parallel to switches  $S_{H2}$  and  $S_{H4}$  are forward biased and positive group switches  $S_{H1}$  and  $S_{H3}$  are ON) and vertical switches (negative group switches  $S_{N1}$  and  $S_{N2}$  are ON). So the battery voltage

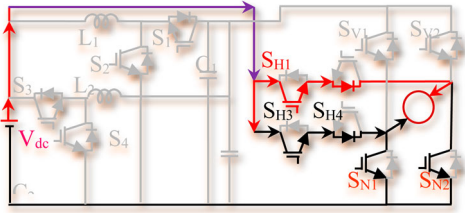


Figure 6. Direct inversion.

from source  $V_{DC}$  is converted into  $V_{AC}$  in the ratio of 1:1, which is filtered and finally connected to grid or R load. The output voltage across  $V_{AC}$  and the equation is given by (Figure 6)

$$V_{AC(rms)} = \frac{2 \times 4V_{DC}}{\pi \sqrt{2}} \quad (3)$$

RMS value of output voltage  $V_{AC}$  and the equation is given by

$$V_{AC(rms)} = \sqrt{\frac{2}{\pi}} \int 2 \times V_{DC}^2 d\theta \quad (4)$$

Fourier series of output voltage  $V_{AC}$  and the equation are given by  $V_{AC(rms)}$  = RMS value of output voltage and  $V_{DC}$  = Input DC voltage to the inverter

$$V_{AC(rms)} = \sum_{n=1,3,5,\dots}^{\infty} \frac{2 \times 4V_{DC}}{n\pi} \sin(n\omega t) \quad (5)$$

### 2.3. Two-stage step-down rectifier operation

Two-stage step-down rectifier operation involves only vertical switches (positive group switches  $S_{V1}$  and  $S_{V3}$  and diode anti-parallel to negative switches  $S_{N1}$  and  $S_{N2}$  are forward-biased), and blue colour DC-DC converter has a provision to step-down voltage to the required level. Diodes anti-parallel to the switches  $S_{V1}$  and  $S_{N2}$  are forward biased during the positive half cycle, and diodes across switches  $S_{V2}$  and  $S_{N1}$  are forward biased during the negative half cycle. So, the alternating current from source  $V_{AC}$  is converted into DC voltage  $V_H$  is in the ratio of 1:1, which is given to blue colour DC-DC converter. DC-DC converter operation is split into two intervals: duty interval and freewheeling interval. During duty interval switch  $S_1$  ON, inductor  $L_1$  sharing voltage with battery, so the voltage across battery  $V_{DC}$  is equal to  $V_L$ . For a freewheeling interval of operation switch,  $S_1$  is turned OFF, so the energy stored in the inductor  $L_1$  is freewheeling via diode anti-parallel to the switch  $S_2$ . Average output voltage during rectification mode with R load is expressed in Equation (6), and RMS output voltage is given in (7) (Figure 7)

$$V_{DCavg} = \frac{2V_m D}{\pi} \cos\alpha \quad (6)$$

$$V_{DCrms} = \frac{V_m D}{\sqrt{2}} \quad (7)$$

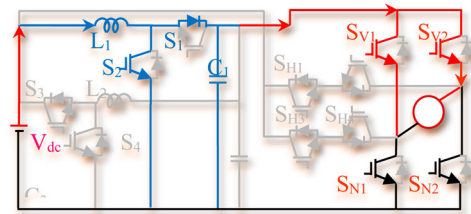


Figure 7. Dual-stage step-up.

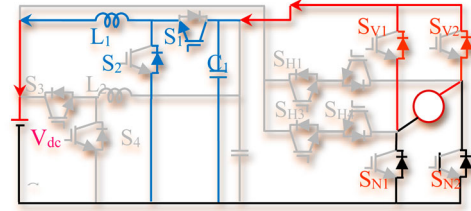


Figure 8. Dual-stage step-down rectification.

### 2.4. Two-stage step-up inverter operation

Two-stage step-up inverter operations first stage conversion is from the blue colour DC-DC converter. The DC-DC converter is a step-up battery voltage  $V_{DC}$  ( $V_L$ ) to the required level  $V_H$ . This operation is split into two intervals: charging interval and duty interval. During charging interval switch  $S_2$  ON, inductor  $L_1$  current linearly increasing from  $I_{Lmin}$  to  $I_{Lmax}$ , so the voltage across capacitor  $C_1$  is stepped-up voltage  $V_L$ . For duty interval of operation switch,  $S_2$  is turned-OFF, so the energy stored in the inductor  $L_1$  is added with source voltage  $V_{DC}$  appears across  $C_1$  due to diode anti-parallel to the switch  $S_1$  is forward biased. Voltage  $V_L$  is input to the vertical inverter for the second stage of conversion, so DC-AC conversion takes place from vertical switches (positive group switches  $S_{V1}$  and  $S_{V2}$  and negative group switches  $S_{N1}$  and  $S_{N2}$ ).  $S_{V1}$  and  $S_{N2}$  are ON to get a positive half cycle, and  $S_{V2}$  and  $S_{N1}$  are ON to get a negative half cycle. So the battery voltage from source  $V_{DC}$  is converted into  $V_{AC}$  in the ratio of 1:2 approximately, which is filtered and finally connected to the grid or R load (Figure 8).

The output voltage across  $V_{AC}$ , and the equation is given by

$$V_{AC(rms)} = \frac{2 \times 4V_{DC}}{\pi \sqrt{2} (1-D)} \quad (8)$$

RMS value of output voltage  $V_{AC}$  and the equation are given by

$$V_{AC(rms)} = \sqrt{\frac{2}{\pi}} \int 2 \times V_L^2 d\theta \quad (9)$$

Fourier series of output voltage  $V_{AC}$  and the equation are given by

$$V_{AC(rms)} = \sum_{n=1,3,5,\dots}^{\infty} \frac{2 \times 4V_L}{n\pi} \sin(n\omega t) \quad (10)$$

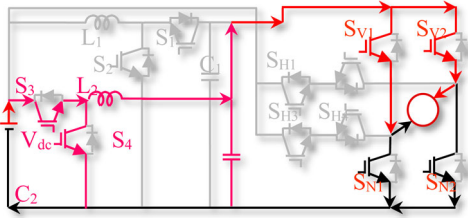


Figure 9. Dual-stage step-down inversion.

### 2.5. Two-stage step-up rectifier operation

First stage  $V_{AC}$  is converted into DC voltage  $V_H$  in the ratio of 1:1 is similar like the previous section, rectifier output is given to pink DC-DC converter is step-up rectifier voltage  $V_L$  to required level  $V_B$ . This step-up operation is also split into two intervals: charging interval and duty interval. During charging interval switch  $S_4$  is ON, inductor  $L_2$  current linearly increasing from  $I_{L2min}$  to  $I_{L2max}$ , so the voltage across the battery is stepped-up voltage  $V_B$ . For duty interval of operation switch,  $S_4$  is turned-OFF, so the energy stored in the inductor  $L_2$  is added with source voltage  $V_L$  appears across battery due to diode anti-parallel to the switch  $S_3$  is forward biased. Voltage  $V_B$  is input to battery charging. Average output voltage during overall rectification mode with R load is expressed in Equation (11), and RMS output voltage is given in (12) (Figure 9)

$$V_{DCavg} = \frac{2V_m}{\pi(1-D)} \cos\alpha \quad (11)$$

$$V_{DCrms} = \frac{V_m}{\sqrt{2(1-D)}} \quad (12)$$

### 2.6. Two-stage step-down inverter operation

Two-stage step-down inverter operations first stage conversion is from the pink colour DC-DC converter. The DC-DC converter is a step-down battery voltage  $V_B$  to the required level  $V_H$ . Pink color DC-DC converter operation is split into two intervals: duty interval and freewheeling interval. During duty interval switch  $S_3$  ON, inductor  $L_2$  sharing voltage with battery, so the voltage across battery  $V_{DC}$  is equal to  $V_L$ . For the free-wheeling interval of the operation switch,  $S_3$  is turned OFF, so the energy stored in the inductor  $L_1$  is free-wheeling via diode anti-parallel to the switch  $S_4$ . The remaining second stage DC-AC conversion is similar to the previous section. The output voltage across  $V_{AC}$  and the equation is given by (Figure 10)

$$V_{AC(rms)} = \frac{2 \times 4 \times DV_{DC}}{\pi \sqrt{2}} \quad (13)$$

RMS value of output voltage  $V_{AC}$  and the equation is given by

$$V_{AC(rms)} = \sqrt{\frac{2}{\pi} \int 2 \times V_H^2 d\theta} \quad (14)$$

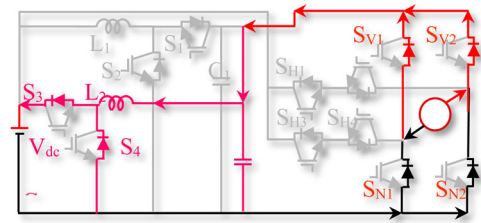


Figure 10. Dual-stage step-up rectification.

Fourier series of output voltage  $V_{AC}$  and the equation are given by

$$V_{AC(rms)} = \sum_{n=1,3,5,\dots}^{\infty} \frac{2 \times 4 \times DV_B}{n\pi} \sin(n\omega t) \quad (15)$$

## 3. CBPWM strategy

The proposed inverter modulation strategy is based on carrier-based pulse width modulation, which is the key factor in evaluating power flow in the DC-DC converter-based three-level DC-AC converter. The modulation technique applied to a conventional converter is entirely different. Owing to its efficiency for practical use, the CBPWM technique for the proposed inverter, which is the primary subject of this article, will be studied. Whenever the conventional CBPWM technique is applied to the proposed converter, dual carriers are symmetrically relocated regarding zero. Power flow direction and voltage balancing of the proposed converter are based on dividing capacitors, which result in the maximum value of carriers. Conversely, for a three-level converter, it is not always true so because the voltage of LV port  $V_L$  is varied. The maximum average values of carriers can differ according to the voltages of  $V_L$  and  $V_H$  when the CBPWM method is implemented in the proposed converter. The magnitudes of the two carriers are proportional to the dc voltage  $(V_H - V_L)$  and  $V_L$ , respectively, as shown in Figure 11, and it can be generalized by Equations (16) and (17).

$$V_m = \frac{(V_H - V_L)}{V_H/2} \quad (16)$$

$$V_m = \frac{2 V_L}{V_H} \quad (17)$$

CBPWM is derived from zero-sequence generators, and asymmetrical carrier wave is shown in Figure 12(a,b) illustrates the waveform for the proposed CBPWM.

$$V_{AC} = \Delta \cos\theta \quad (18)$$

The modulation process of DC-AC converter is to optimize the power at lower level  $P_{Low}$ , which is transmitted directly within the sole operating point from the low voltage port to grid. The key step is power flow analyzing the proposed converter, which is to deduce the

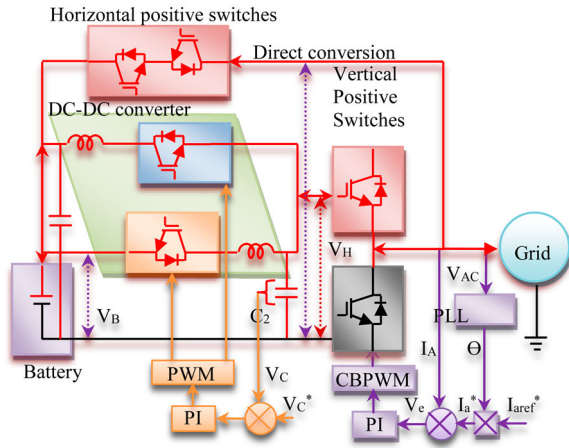


Figure 11. Control strategy.

average current flowing from the DC-AC converter’s LV port, defined as  $I_L$ , CBPWM of the proposed modulation scheme is shown in Figure 12. It is important to raise the average  $I_L$  value to optimize the real power that is directly supplied to the grid with single-stage power conversion. Finally, it stops current flow in the whole pulse period of the low-voltage port is to enable the duty ratio when the state current is null. DC-AC converter current is calculated in the following Equation (19). Comparison and components parameters are given in Table 1.

$$I_{AC} = I_m \cos(\theta - \varphi) \tag{19}$$

4. Analysis of active power and characteristics

Power from the energy storage device, which is directly supplied to the load, is expressed in (20)

$$P_{Low} = V_L \frac{1}{2\pi} \int_0^{2\pi} i_{AC}(\theta) d\theta \tag{20}$$

$$P_{Low} = V_L \frac{1}{2\pi} \int_0^{2\pi} (Di_{AC})(\theta) d\theta \tag{21}$$

Power in phase is expressed in (22)

$$P_L = V_L \frac{1}{2\pi} \int_0^{2\pi} (Di_{AC})(\theta) d\theta \tag{22}$$

Zero sequence components of the proposed CBPWM during the interval of  $0^\circ$ – $180^\circ$  are given as (23)

$$V_{AC}^I = \Delta \cos\theta - 30^\circ - 1 \tag{23}$$

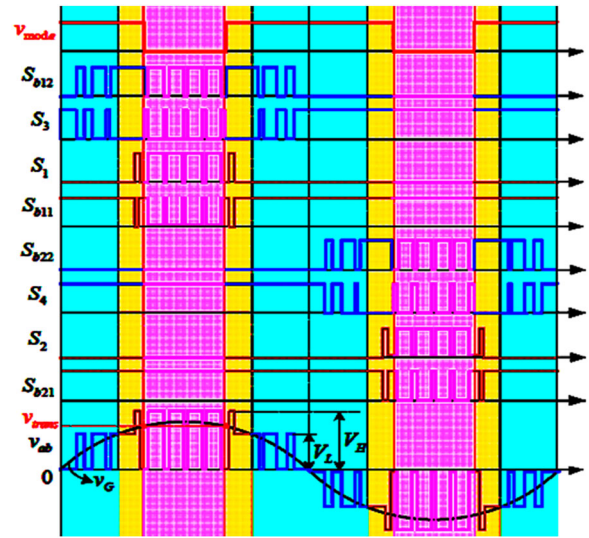


Figure 12. Proposed converter switching waveform.

5. Hardware experiment

A prototype model developed based on the proposed concept with a power rating of 250 W is illustrated in Figure 13. The proposed idea is to verify in practical using theoretical analysis. DC-DC converter voltage is (20–50) V is connected with ESD. The maximum range of AC side (grid side) voltage is 230 V. Switching frequency of the converter switches is 50 kHz, turns ratio (K) is designed as 5/25, resonance inductance is selected as 50  $\mu$ H, IGBTs’ IRBF2207b is used, and capacitance value is 2  $\mu$ F and DC side capacitance is 7 mF.

Steady-state voltage 20 V at the power of 250 W is obtained during full load, as shown in Figure 14. Input voltage is small during the step-down mode, and the step-up modems is control output current. Due to parasitic capacitance in the switches, AC-DC mode voltage is higher than DC-AC voltage. Zero voltage transition is achieved during full load, and its performance is tested at an input voltage of 20 V in the DC-AC mode. The driving signal of the DC-DC converter is as shown in Figure 14. Grid voltage in the output side of the inverter is as shown in Figure 15.

During the step-down mode, the current lags voltage, so the output side easily achieves this zero voltage switching. During boost or step-up mode of operation switch,  $Q_5$  is turned ON three times in each switching period; due to resonance switch,  $Q_5$  can operate with

Table 1. Comparison of components and parameters.

Parameters	5L-ANPC	5L-UGANPC	C-QSBI	E-QSBI	SL-QSBI	TZSI	QTSI	ASTS-BI	VVS-DC link	Proposed converter
Switches	7	8	9	7	7	7	6	6	8	8
Diodes	2	–	–	8	8	11	7	7	8	8
Capacitors	3	3	3	1	1	1	1	2	1	2
Inductor	1	1	1	1	1	1	1	1	1	2
Switching stress	High	High	Low	High	High	High	High	Low	Low	Low
Max. switch current	$I_L$	$I_C$	$I_C$	$I_C$	$I_C$	$I_C$	$I_L$	$I_L$	$I_L$	$I_C$
Max. switch voltage	110	110	220	220	75	100	100	100	200	220

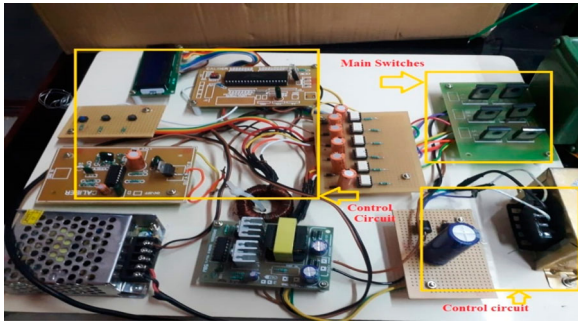


Figure 13. Hardware prototype model.

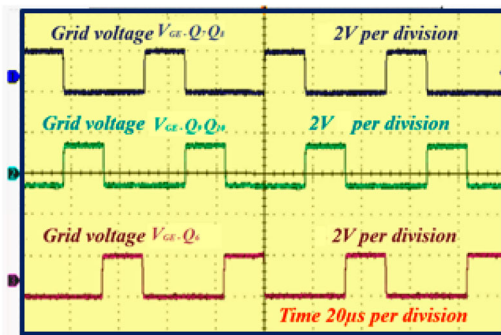


Figure 14. Driving signal.

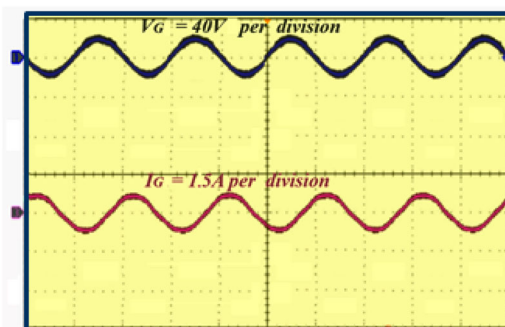


Figure 15. Grid voltage in the output side.

zero current sources gate signal, as shown in Figure 15. Dynamic performance of the proposed converter mode transition between DC-AC and AC-DC mode is tested at maximum voltage point of  $V_G$ . Prototype result load step under AC-DC mode is shown in Figure 16; it is seen power flow is quickly changed from the DC-AC to AC-DC mode. The transition from the AC-DC mode to the DC-AC mode is illustrated in Figures 17 and 18.

Efficiency is calculated at different loads and compared with existing converters as shown in Figure 19. Theoretical-practical efficiency comparisons are made, as shown in Figure 20. The transferred power sign is positive, the proposed converter is in the DC-AC mode or the AC-DC mode. Full load efficiency is 93.6%, and maximum efficiency of 97.4% is obtained when power is 100W i.e. 40% of total load during the AC-DC mode. THD (Total Harmonic Distortion) of current is tested, while the converter works as DC-AC and AC-DC, as shown in Figure 21. If the output power is

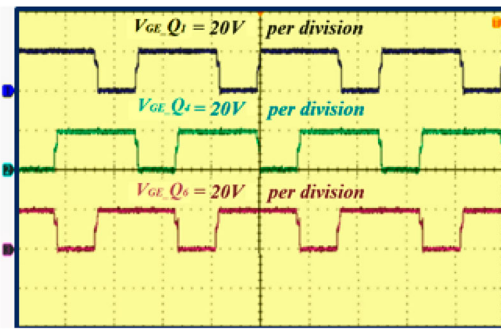


Figure 16. Gate signal of DC-AC converter.

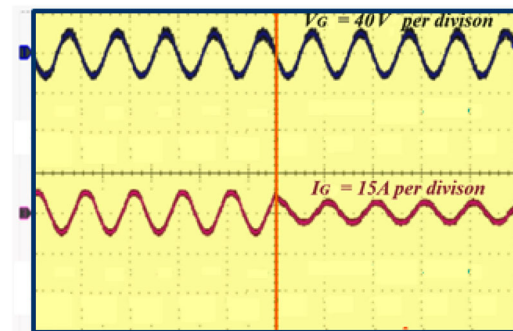


Figure 17. AC-DC mode with different loads.

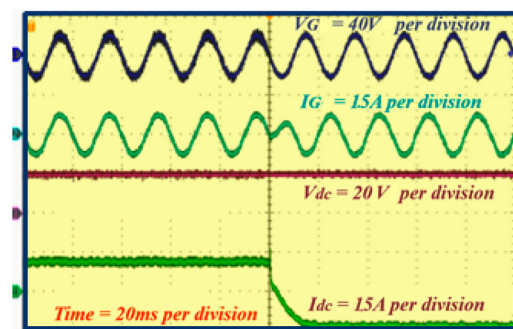


Figure 18. Transition from AC-DC mode to DC-AC mode.

Table 2. Parameter comparison.

Parameters	Traditional converter	Proposed converter
DC side voltage	25–40 V	20–50 V
AC side grid voltage	220 V	230 V
Frequency	50 Hz	50 Hz
Power output	200 W	300 W
Switching frequency	50 kHz	50 kHz
Efficiency	96.9%	97.9%
THD full load	2.6–3.3%	2.3–3.3%

greater than 60% THD. The obtained value is 4.5% during both modes of operation. The proposed converter practically achieved a THD value of 2.3%. Comparison between traditional and proposed converters [11] is given in Table 2. Efficiency and THD values show the proposed converter with a prototype model is better than a traditional converter.

The tested findings are displayed in Figures 15–20, where it is clear that the suggested converter may

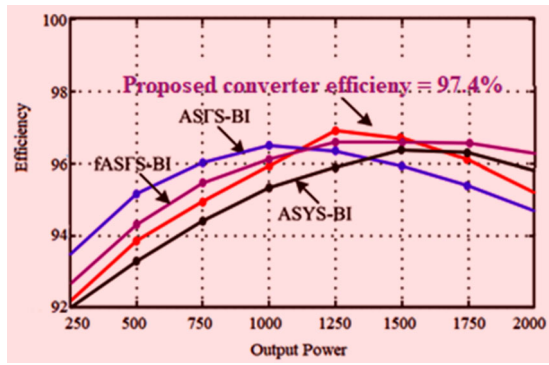


Figure 19. Efficiency vs. Power at different loads.

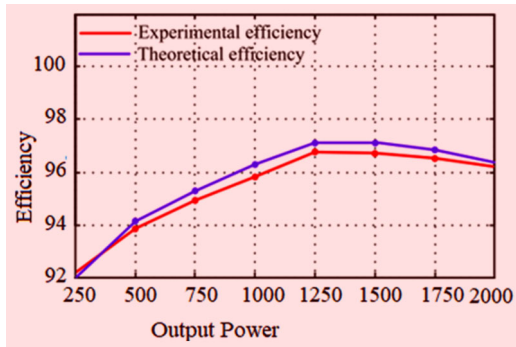


Figure 20. Efficiency comparison.

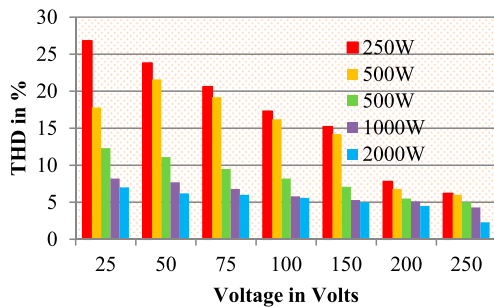


Figure 21. THD values from different powers.

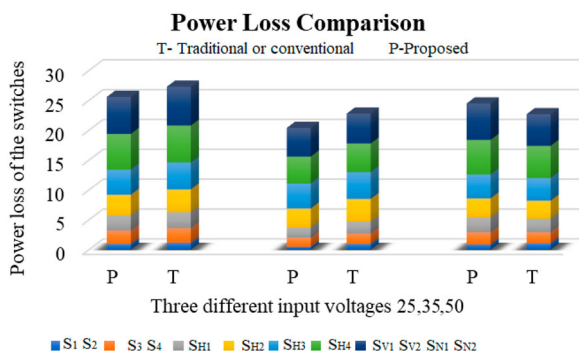


Figure 22. Switching power loss comparisons.

achieve substantially better efficiency than typical converters. The suggested converter’s active switches and the typical two-stage converter’s power loss breakdown are computed and displayed in Figure 22.

## 6. Conclusion

This paper proposed single-phase isolated BHC based on IPWM controlled resonant converter and verified it with an energy storage system. With IPWM, controlled conversion is achieved with a wide voltage range in step-up and step-down modes. The proposed control magnitude and time are suddenly changed with smooth switching operation. Prototype 2000 W with a voltage range of 25–250 and 230 V RMS is implemented to verify the output. The proposed TBC has achieved a maximum efficiency of 97.4%, and the obtained THD is 2.3%.

## Disclosure statement

No potential conflict of interest was reported by the author(s).

## References

- [1] Narimani M, Moschopoulos G. An investigation on the novel use of high-power three-level converter topologies to improve light-load efficiency in low power DC/DC full-bridge converters. *IEEE Trans Ind Electron.* 2014;61(10):5690–5692.
- [2] Wu T-F, Chen Y-K. Modeling PWM DC/DC converters out of basic converter units. *IEEE Trans Power Electron.* 1998;13(5):870–881.
- [3] Ayachit A, Kazimierczuk MK. Averaged small-signal model of PWM DC–DC converters in CCM including switching power loss. *IEEE Trans Circuits Syst Express Briefs.* 2019;66(2):262–266.
- [4] Kim K, Cha H, Park S, et al. A modified series-capacitor high conversion ratio DC–DC converter eliminating start-up voltage stress problem. *IEEE Trans Power Electron.* 2018;33(1):8–12.
- [5] Pesce C, Blasco R, Riedemann J, et al. A DC–DC converter based on modified flyback converter topology. *IEEE Latin Am Trans.* 2016; 14(9):3949–3956.
- [6] Guo Z, Li H, Liu C, et al. Stability-improvement method of cascaded DC–DC converters with additional voltage-error mutual feedback control. *Chinese J Electr Eng.* 2019;5(2):63–71.
- [7] Yang L, Liang T, Chen J. Transformer less DC–DC converters with high step-up voltage gain. *IEEE Trans Ind Electron.* 2009;56(8):3144–3152.
- [8] Ye Y, Zhou K, Zhang B, et al. High-performance repetitive control of PWM DC–AC converters with real-time phase-lead FIR filter. *IEEE Trans Circuits Syst Express Briefs.* 2006;53(8):768–772.
- [9] Sayed MA, Suzuki K, Takeshita T, et al. Soft-switching PWM technique for grid-tie isolated bidirectional DC–AC converter with SiC device. *IEEE Trans Ind Appl.* 2017;53(6):5602–5614.
- [10] Sayed MA, Takeshita T, Kitagawa W. Advanced PWM switching technique for accurate unity power factor of bidirectional three-phase grid-tied DC–AC converters. *IEEE Trans Ind Appl.* 2019;55(6):7614–7627.
- [11] Sundaramoorthy P, Balaji M, Suresh K, et al. Prototype implementation for vibration analysis in circuit coupled E-core flux reversal free stator switched reluctance motor drives. *Circuit World.* 2020;46(4):325–334.
- [12] Venkatesan M, Adhavan B, Suresh K, et al. Research on FPGA controlled three phase PV inverter using multi

- carrier PWM control schemes. *Microprocess Microsyst Elsevier*. 2020;76, July 2020, Article 103089.
- [13] Saravana Ram R, Lordwin cecil Prabhaker M, Suresh K, et al. Dynamic partial reconfiguration enhanced with security system for reduced area and low power consumption. *Microprocess Microsyst Elsevier*. 2020;76, July 2020, Article 103088.
- [14] Suresh K, Jyotheeswara Reddy K, Dash R, et al. A universal converter for different power conversion operations and high power applications. In *2021 IEEE 12th Energy Conversion Congress & Exposition – Asia (ECCE-Asia)*; 2021. p. 1666–1671.
- [15] Pothuraju P, Subbarao M, Suresh K. Design and analysis of grid tied renewable energy system based e-chopper using main controller. *J Europ Syst Autom*. 2020;52-6:225–237.
- [16] Ji Y, Geng L, Li F, et al. Active-switched coupled-inductor impedance network boost inverters. *IEEE Trans Veh Technol*. Jan. 2021;70(1):319–330.
- [17] Lee SS, Lim CS, Lee K. Novel active-neutral-point-clamped inverters with improved voltage-boosting capability. *IEEE Trans Power Electron*. 2020;35(6): 5978–5986.
- [18] Suresh K, Vijayshankar S, Sathyaseelan B, et al. Multi-input multi-output converter for universal power conversion operation. *J Circuits Syst Comput* . 2021;36(6): 6192–6196.